Hydro-mechanical behaviour of a cement-bentonite mixture along evaporation and water-uptake controlled paths

Hydro-mechanical behaviour of a cement-bentonite mixture along evaporation and water-uptake controlled paths

Guido Musso[1], Vincenzo Sergio Vespo[1], Giulia Guida[2], and Gabriele Della Vecchia[3]

[1]Politecnico di Torino, Dipartimento di Ingegneria Strutturale, Edile e Geotecnica (DISEG)

[2]Università degli Studi di Roma Tor Vergata, Dipartimento di Ingegneria Civile e Ingegneria Informatica (DICII), formerly Politecnico di Milano

[3]Politecnico di Milano, Dipartimento di Ingegneria Civile e Ambientale (DICA)

Abstract

The results of a laboratory investigation on the effects of drying and wetting on the hydro-mechanical behaviour of a cement-bentonite mixture are presented. A large hysteresis along the hydraulic paths was found for what concerns both the water retention and the volume strains. This might be related to the shrinkage of cement bentonite clusters and to the development of micro-cracks, that were observed with a microscope along drying. Macroscopic cracks developed in a squat sample which had been cured for 28 days and was then left to dry in the laboratory environment, while this did not occur in an analogous sample cured for 60 days, possibly in virtue of its higher strength as detected through a pocket penetrometer. Water uptake after partial desaturation of squat and column samples took place in short times with respect to drying, but it did not allow for a full recovery of the initial water content. Electrical Resistivity Tomography (ERT) monitoring provided reliable water content determinations in the high range and correct indication of crack patterns at low water contents. A good reproduction of the experimental results was obtained with a coupled Thermo-Hydraulic model formulated on purpose.

1 Introduction

Cement-bentonite mixtures (CB) are widely employed in many geotechnical and geo-environmental applications such as jet grouting, pile systems and slurry trench cutoff walls. The latter aim at controlling groundwater flow and at confining both dissolved and non-aqueous pollutants (Cermak *et al.*, 2012; Evans and Ruffing, 2017). Cutoff walls are generally built excavating trenches enclosing the polluted site, and filling them up with the CB slurry (Ryan, 1985; Evans, 1994; Malusis *et al.*, 2017). The curing process, that occurs on site, conveys to the mixture target properties in terms of hydro-mechanical behaviour and durability (Fratalocchi *et al.*, 2006; Guida *et al.*, 2021; Flessati *et al.*, 2021).

In many site applications, the water level inside or outside the encapsulated area may fluctuate over time due to natural and anthropogenic causes. Furthermore, the top of the wall is exposed to the atmosphere, being subjected to evaporation (whose effects will be increasingly important due to climate change) or infiltration processes. As a consequence, a significant part of the barrier may be subjected to drying/wetting cycles (Wu *et al.*, 2019). This may lead to changes in the hydraulic state of the material and to a reduction of the overall effectiveness of the barrier (Malusis *et al.*, 2011).

In particular, the shallower portions of cutoff walls often show signs of damage due to drying soon after the construction, especially if they are left uncapped (Joshi *et al.*, 2009). According to Jefferis (2012), CB slurry trench cutoff walls develop desiccation cracks because of drying induced shrinkage. The formation of cracks affects the transport properties required for a good performance of the barrier, leading *e.g.* to an increase of hydraulic conductivity of about 2-3 orders of magnitude, to a degradation of material strength and to an increase in heterogeneity of the wall on site (Joshi *et al.*, 2009; Wu *et al.*, 2019). Despite the engineering relevance of the changes in hydraulic properties that might be triggered by desiccation, a limited number of studies has been focusing on these aspects. Soga *et al.* (2013) found that CB samples cracked when exposed to laboratory air, but remained intact when they were immersed in a box filled with sand and then exposed to drying-wetting cycles. (Royal *et al.*, 2018) have reported experimental evidences about microstructural changes of enriched cement-bentonite specimens exposed to air, including discolouration (changing from dark green to a very pale blue tinged light grey), formation of irreversible drying induced shrinkage cracks on the surface, widening (and intersection) of cracks with prolonged drying upon complete disgregation. A few studies dealt with the effects of additives on the tendency to cracking of the cement bentonite mixtures. The ash of slag enrichment allows to improve the low permeability requirements for the CB in saturated conditions, but it seems to induce worse performances upon drying (Jefferis, 2012), whereas according to the experimental evidence in Cao *et al.* (2021) adding super-absorbent poly-

mers increases the resistance to cracking of the mixture.

In general, a full understanding of the impact of evaporation and infiltration, and therefore of drying and wetting cycles, on the hydro-mechanical behaviour of CB mixtures is still missing. As an attempt to contribute to this aspect, obtained through the material characterization aimed at thermo-hydraulic modelling, this paper presents the results of a laboratory study on the hydro-mechanical behaviour of CB samples in unsaturated conditions, with a focus on the water retention properties and on the volumetric and strength changes induced by suction variations. No additives were used in the preparation of the mixtures used in this study, as this can be considered the 'baseline' material with respect to whom the enriched mixtures might be compared. Royal *et al.* (2018) have reported experimental evidences about microstructural changes of enriched cement-bentonite specimens exposed to air, including discolouration (changing from dark green to a very pale blue tinged light grey), formation of irreversible drying-induced shrinkage cracks on the surface, widening (and intersection) of cracks with prolonged drying upon complete disgregation.

The effects of suction changes on the water retention and on the volumetric behaviour were investigated first. A preliminary insight on the effects of water content on strength was obtained through pocket penetrometer measurements, while the development of cracks along drying was checked with visual inspection and Electrical Resistivity Tomography (ERT) on squat samples. Evaporation and water uptake from a column sample was investigated assessing local changes in the water content through ERT. A good reproduction of the results of the drying and water uptake experiments was obtained through simulations with a Thermo-Hydraulic coupled model, whose parameters were set up accordingly with the previous water retention and permeability measurements .

2 Material and methods

2.1 Material

The tests were performed at the Geotechnical Engineering Lab of the Department of Structural, Geotechnical and Building Engineering of Politecnico di Torino. CB mixtures were prepared by mixing a commercial cement (CEM I 32.5 N, Portland 325) with a commercial mixed sodium-calcium bentonite provided by Laviosa Chimica Mineriaria (Livorno, Italy). The bentonite has a liquid limit w_L = 616%, a plastic limit w_P = 42%, a specific gravity G_s = 2.95 and a powder hygroscopic water content at laboratory conditions w = 14% (Trischitta *et al.*, 2020). The mixing proportions are consistent with the ones used in the construction of the cuf-off walls (see *e.g.* Sarsby 2013). The mixture

preparation procedure consisted in: (i) mixing tap water with bentonite at a 18:1 water-bentonite mass ratio until a homogeneous plastic slurry was obtained; (ii) leaving the slurry covered with an impermeable sheet for 24 hours to ensure full hydration; (iii) adding dry cement powder in order to obtain a cement-bentonite mass ratio 4:1 and stir again the suspension; (iv) pouring the mixture into plastic cylindrical moulds of different size and leaving it to cure immersed in tap water for 28 or 60 days. The specific gravity of the endured mixture was $G_s = 2.68$. The water content of the samples was found to range between $w_0 = 285\%$ and $w_0 = 325\%$, while the saturated hydraulic conductivity at a confinement of 50 kPa measured with flexible and rigid wall permeameters was around $K_w^{sat} = 10^{-8}$ m/s.

2.2 Water retention determinations

Four different techniques (axis translation, filter paper, vapour equilibrium VET and measurements with a WP4 dewpoint psychrometer) were employed to determine the water retention properties of the CB mixture. The main drying branch of the water retention was determined exposing specimens extracted from the curing bath to increasingly high suctions, whereas the main wetting branch was determined by exposing specimens that had been previously dried in the laboratory environment (fixed temperature of T=21 °C and relative humidity $h_r = 0.38$) to progressively lower suctions.

The axis translation (Hilf, 1956) and the filter paper techniques (ASTM, 2016) were used either to impose or measure matric suction s. The axis translation technique was implemented in a suction controlled oedometer and the range of suction explored was 0.050 MPa $\leq s \leq$ 0.30 MPa. Different values of air and water pressures were imposed independently while the volume of water leaving or entering the specimen was measured with a volume indicator. The height of the specimen was monitored with a LVDT. The filter paper technique was implemented using the Scheicher & Schuell no. 589 WH filter paper: the range of suction explored was 0.020 MPa $\leq s \leq$ 2 MPa. Two twin specimens were used for each determination: along the drying path, they were partially dried through exposure to the laboratory air; along the wetting path, fully dried specimens were partially wetted adding known masses of water. Three sheets of filter paper were sandwiched between the specimens and the whole assemblage was sealed hermetically in plastic containers for 15 days before the mass and suction determinations. Changes in size were measured with a calliper.

Vapour Equilibrium technique (VET) and a WP4 dewpoint psychrometer (Decagon Devices) were adopted either to impose or measure total suction ψ. The VET was used over a range 9.60 MPa $\leq \psi \leq$55 MPa, suspending the specimens in hermetically closed jars above saturated salt solutions.

Changes in the mass of the specimens were measured with a high precision balance and occurred in about 2-3 weeks. Measurements of ψ with the WP4 were taken on specimens that, after exposure to the laboratory environment or addition of water, had been sealed in plastic covers and suspended above pure water for 48 hours to allow for suction homogenization. The mass of the specimens was measured with a high precision balance and their size was measured with a calliper. However, for suctions $\psi > 14$ MPa the specimens became very fragile and use of the calliper impossible. Some of the specimens cracked at high suctions. In this case, where possible, measurements were performed on their larger surviving portions. In this sense, the provided water retention characterization refers to the hydraulic properties of the cement bentonite matrix.

The matric suction of the VET and WP4 measurements was determined as:

$$s = \psi - \pi \tag{1}$$

where π is osmotic suction, which in diluted solutions is linearly proportional to the concentration of species dissolved in the pore water. The osmotic suction at different water contents was evaluated as:

$$\pi = \pi_0 \frac{w_0}{w} \tag{2}$$

w_0 and w being the initial and the current water content and π_0 being the osmotic suction of the curing bath, approximately equal to 285 kPa according to WP4 measurements. Note that the relatively high value of π_0 has to be related, at least partially, to the dissolved species present in the bentonite powder and to the reaction products of the hydration of the cement.

2.3 Microstructural determinations

Microstructural effects induced by relatively high suctions on specimens cured for 28 days were investigated by means of Scanning Electron Microscopy (SEM) analyses. Three conditions were investigated: fully saturated ($s = 0$ MPa, specimen as extracted by the curing bath), dry ($s \simeq 129$ MPa, induced by drying at the laboratory conditions) and at an intermediate suction ($s \simeq 4$ MPa, obtained conditioning the specimen with the VET). The specimens, with the exception of the dry one, were preliminarily freeze-dried to avoid undesired changes in the microstructure due to oven drying (see *e.g.* Delage and Pellerin 1984).

2.4 Strength determinations

A preliminary characterization of the effects of suction/water content on the strength of the CB samples was pursued measuring the tip resistance of a pocket penetrometer during sample drying. The values of resistance reported in the following are the average of three determinations. A commercial pocket penetrometer from Controls with a range 0-5 MPa was used.

2.5 Electrical conductivity and ERT reconstructions

Electrical Resistivity Tomography (ERT) is a technique that allows the reconstruction of the electrical conductivity field within an object, based on the inversion of electrical measurements performed at the boundaries of the object itself. Injecting and measuring electrodes are needed, and their position is changed until a number of measurements sufficient for the tomographic reconstruction is performed (Borsic *et al.*, 2005). The information provided by the distribution in space and time of the electrical conductivity is very useful for geo-environmental applications: it has been in fact successfully used as a proxy to detect heterogeneities (Borsic *et al.*, 2005), porosity changes, distribution of contaminant in soil samples (Comina *et al.*, 2011), also allowing estimating the water retention and hydraulic properties of different soils (Cosentini *et al.*, 2012). It also has been used to investigate moisture movement in cement, both undamaged (Smyl *et al.*, 2016) – thus allowing to study the homogeneous behaviour of the material matrix – and cracked (Smyl *et al.*, 2017). A 2D reconstruction protocol (as in Musso *et al.* 2020) was set up, relying on measurements taken from 16 electrodes equally spaced along the circumference of the CB samples. Electrodes were thin silver squared foils of approximately 5 mm sides, welded to silver wires. The electrodes were placed inside the moulds before pouring the mixture for curing.

In order to provide a reliable map of water content distribution, a relationship between electrical conductivity and the amount of water in the porous material is needed. Theoretical relationships are available relating the electrical conductivity of rocks and soils to water content, porosity and mineralogy: however, to the authors' knowledge, their validity has not been checked for cement bentonite mixtures and in this study a phenomenological law based on a preliminary characterization was preferred. Such a characterization was performed on cylindrical specimens of height H =80 mm and cross section S =507 mm^2. Two cylindrical electrodes, A and B, were applied at the ends of the cylinders, while two 'needle' electrodes (M and N) were inserted along the side, at a distance L=40 mm one from the other and equally spaced from the ends (scheme of the apparatus in Figure 1).

The electrical conductivity χ was evaluated as:

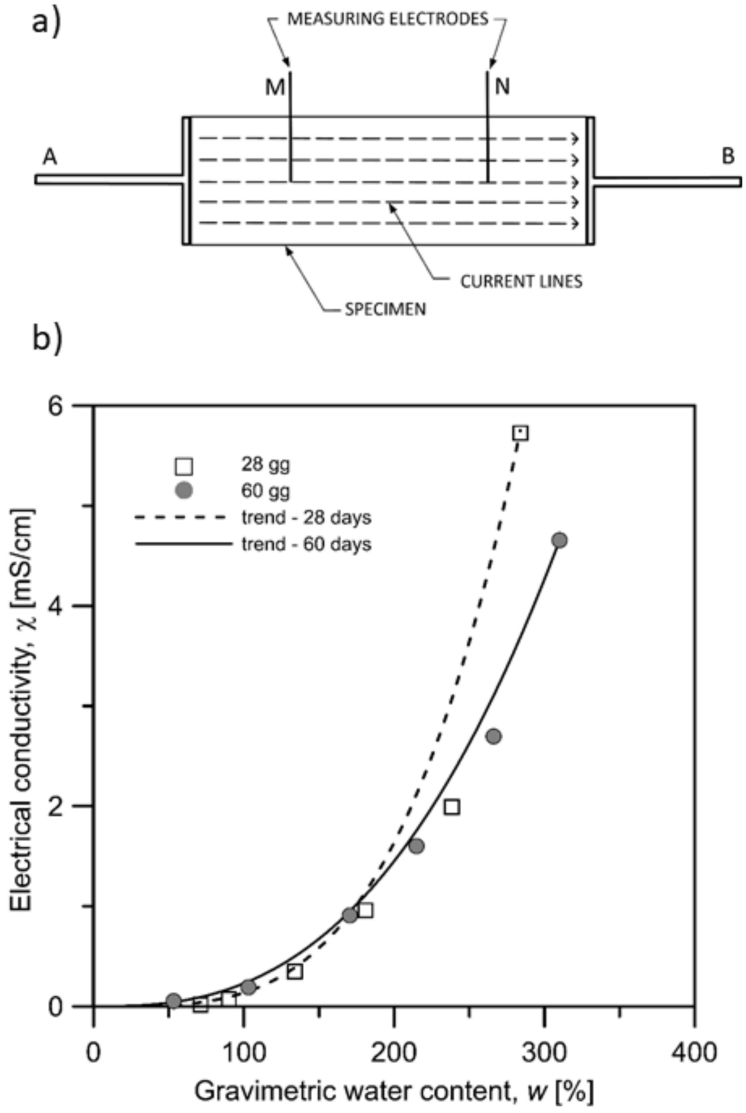

Figure 1: a) scheme of the equipment used for determining the relationship between water content and electrical conductivity b) relationship between water content and electrical conductivity

$$\chi = \frac{\Delta V}{I}\frac{L}{S} \tag{3}$$

where I is the electrical current applied by electrodes A and B and ΔV is the drop of electrical potential between M and N.

The first measurement was performed immediately after removing the specimens from the water bath where they were cured, starting from the initial water content. Other measurements were performed at decreasing water contents after a controlled air drying procedure. The specimens were exposed to the laboratory air for a few hours, then wrapped up in a plastic cover and left to equilibrate in a humid environment for 24 hours (Zibisco, 2019). They were then weighted before a new electrical test. Volume changes were determined with a caliper. The procedure was repeated down

to a water content w = 53%. Lower water contents were not investigated, due to the progressive increase in sample fragility and the large reduction in electrical conductivity. Experimental evolution of electrical conductivity with water content is shown in Figure 1 b. Experimental data are fitted with equation (4):

$$\chi = \chi_0 \left(\frac{w}{w_0} \right)^{\beta} \tag{4}$$

where χ_0 and w_0 are the electrical conductivity and the gravimetric water content of the saturated specimens and β is a parameter that depends on the curing time, equal to 3.59 for 28 days of curing and to 2.66 for 60 days of curing. The electrical conductivity and the water content of the specimens as extracted from the curing bath were respectively χ_0 = 5.75 mS/cm and w_0 = 284 % (28 days of curing), χ_0 = 4.66 mS/cm and w_0 = 310 % (60 days of curing).

3 Water retention and volume changes along drying and wetting

The measured water retention curve for the CB mixture is shown in Figure 2, both in terms of liquid degree of saturation S_l and volumetric liquid content w. The wetting and drying branches of the water retention were fitted by means of the van Genuchten equation (Eq.5):

$$S_l = S_{res} + (1 - S_{res}) \left[1 + (\alpha s)^n \right]^{-m} \tag{5}$$

where S_{res} is the residual degree of saturation and α, n and m are model parameters whose values are reported in Table 1.

Table 1: van Genuchten water retention curve parameters

	main drying	main wetting
α [1/MPa]	0.38	30
n [-]	2.05	0.70
m [-]	0.73	0.60
S_{res} [-]	0.04	0.04

A large hydraulic hysteresis is appreciated in the (S_l,s) plane: along the main drying path the mixture remains nearly saturated up to matric suctions of about s = 800 kPa while along the main wetting path the degree of saturation is as low as S_l = 0.60 for s = 50 kPa. Differences between the main drying and the wetting branches are even larger in the (w,s) plane. This is caused by the volumetric

behaviour of the mixture, shown in Figure 3. Upon drying, changes in the void ratio are very small up to a threshold matric suction of about 4-5 MPa, while a strong shrinkage occurs at higher suctions. Upon wetting from dry conditions swelling is very limited and the volume remains almost constant.

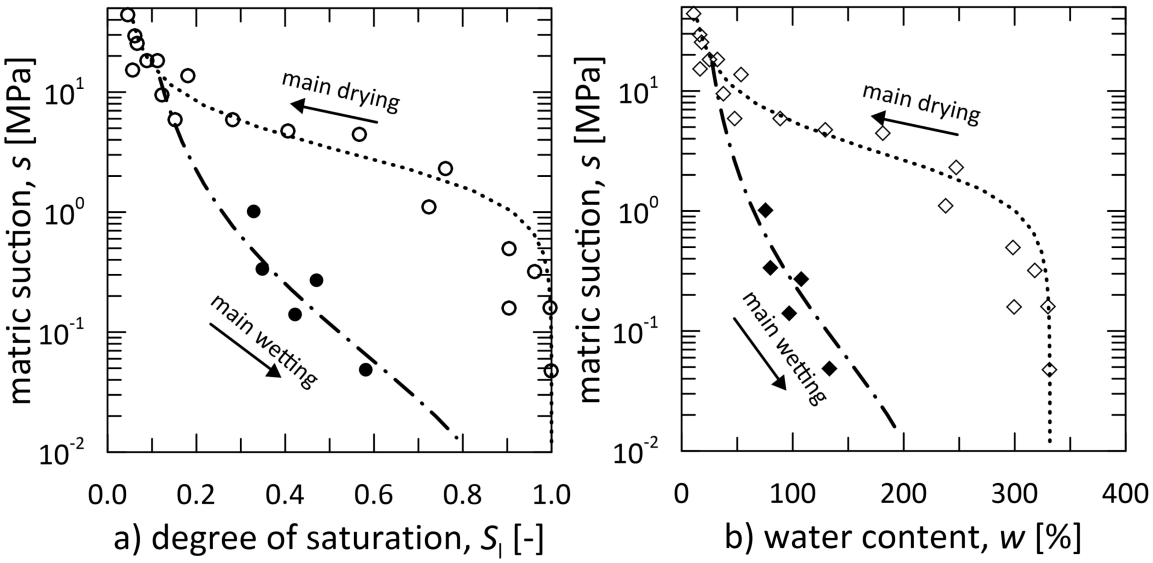

Figure 2: Water retention curves in terms of: a) degree of saturation; b) gravimetric water content.

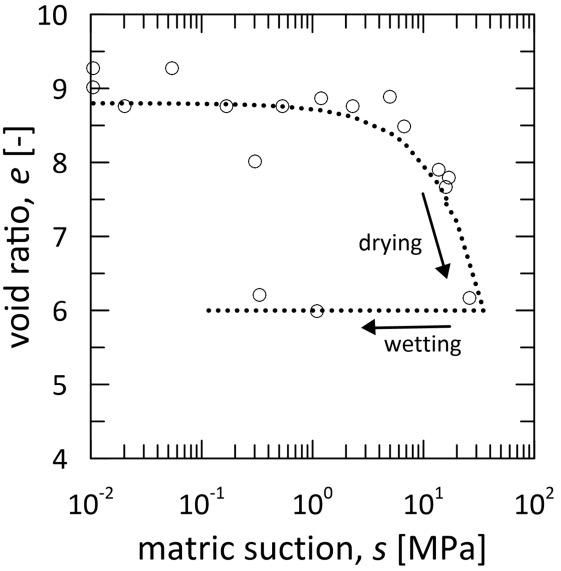

Figure 3: Void ratio evolution along drying and wetting paths

An insight on the microstructural effects which cause such large hydraulic hysteresis and non reversible volumetric behaviour was given by SEM investigations. Figure 4 provides images obtained with a 500 x magnification for a saturated specimen, for a specimen dried to $s \simeq 4$MPa and for a fully dried specimen. The saturated specimen (left) has a quite homogeneous matrix structure, with a uniform distribution of cement-bentonite clusters. The size of these clusters is reduced at $s \simeq 4$ MPa, which causes the onset of micro-cracks with a very small aperture (elongated 'pores' which

run diagonally from the bottom left to the top right of the central image in Figure 4). In fully dry conditions (right image in Figure 4) the CB clusters largely shrank and the micro-cracks enlarged.

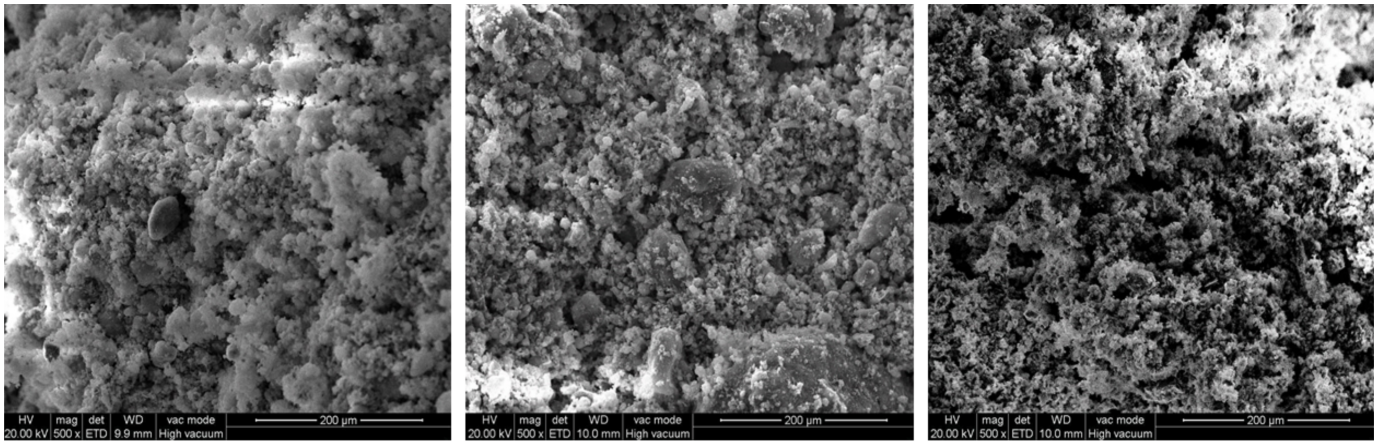

Figure 4: SEM images of: a) saturated specimen; b) specimen equalised at $s \simeq 4$ MPa; c) dry specimen. Bar length is 200 μm in all images

4 Evaporation and water uptake tests

An experimental investigation on the processes related to evaporation and water uptake in CB mixtures was carried out. Tests were run on squat samples with initial height H = 40 mm and diameter D = 110 mm and on a bench-scale column sample with initial height H = 300 mm and diameter D = 130 mm.

The samples were taken out of the curing bath whereas they were kept inside the mould into which they were cured. Evaporation was induced by exposing their top surface to the laboratory environment (temperature $T = 21°$C and relative humidity $h_r = 0.38$, total suction $\psi \simeq 131$ MPa). During the drying stage, stage 1 in the following, they were placed on a plastic surface to which their bottom was sealed. During the water uptake stage (see Figure 5), stage 2 in the following, they were immersed in water for two days (water heigh 10 mm height for the squat samples and 40 mm for the column sample). Test details are reported in Table 2.

4.1 Squat samples

These tests were aimed at checking the use of ERT as a tool for indirect measurements of the water content of CB mixtures, at gaining a qualitative observation of cracking and at obtaining a preliminary evaluation of the relationship between strength and water content, determined with pocket penetrometer measurements during drying. Two different curing times were considered: in the fol-

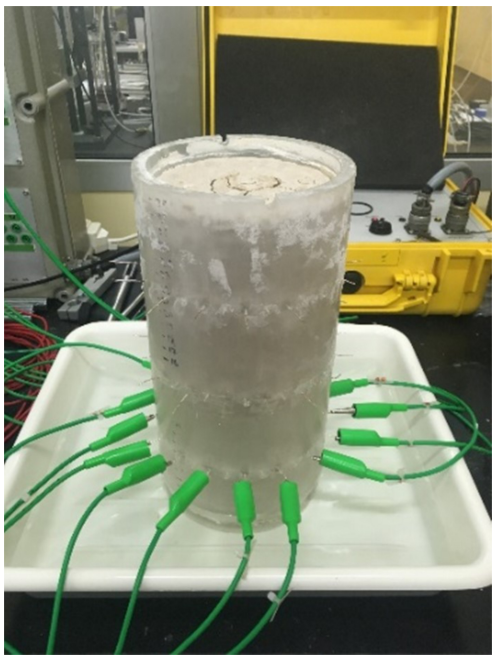

Figure 5: Stage 2 (water uptake) of the experiment on the columnar sample.

Table 2: Details of the evaporation and water uptake tests

	Squat samples		Column sample
	test A	test B	
height [mm]	40	40	300
diameter [mm]	110	110	130
curing [day]	28	60	60
duration of stage 1 [days]	10	8	13
duration of stage 2 [day]	2	2	2
initial void ratio, e [-]	8.05	7.80	6.60 – 8.50

lowing 'test A' stands for 28 days of curing and 'test B' for 60 days of curing. Since pocket penetrometer are destructive measurements, two samples were used for each curing time: one of them for crack detection and ERT, the other one for the penetrometer tests.

The average water content was physically measured by weighting the samples on a high precision balance, while it was also reconstructed by coupling the electrical conductivity maps from the ERT with the equation (4). As shown in Figure 6, loss of water content proceeded quite linearly with time, at a rate that was slightly higher in test B with respect to test A. ERT provided a very good estimate of the average water content for the initial stages of the tests, during which cracking was not detected through naked eye observations and homogeneous maps of water content were obtained (Figure 7).

At longer times (more than 4 days for test A and 7 days for test B) ERT estimations diverged from physical measurements. This mainly occurred because of an increasing number of errors in the electrical measurements due to poor contact between the electrodes and the samples and to crack oc-

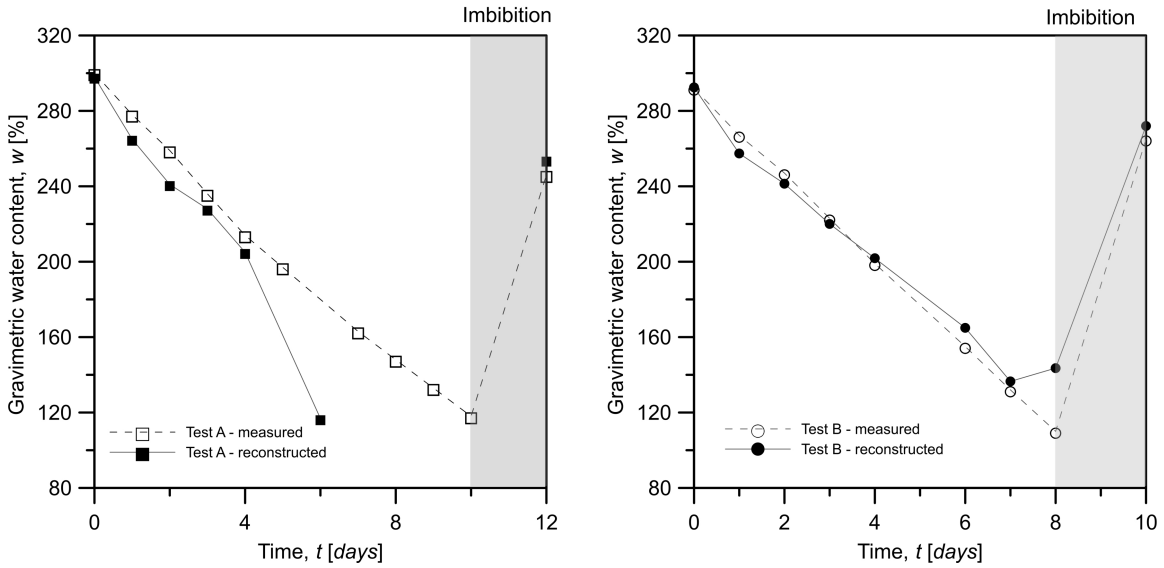

Figure 6: Water content evolution of squat samples during the evaporation and water uptake tests. a) Test A; b) Test B

currence, which started to develop in Test A after about 7 days. The water content was then $w \simeq 160$ % , which according to the water retention in Figure 2 corresponds to a suction $s \simeq 4$ MPa. The state of such sample at the end of the evaporation phase, *i.e.* after 10 days, is presented in Figure 8. While at this point water content estimation proved to be totally unreliable, ERT was still able to detect the crack pattern that had developed as areas of very low electrical conductivity, although the thickness of the discontinuities is not matched. In general, ERT reconstructions were able to detect cracks having a thickness of the order of 2-3 mm. Notice that the thickness of the inclusion that can be matched with the electrical tomography strongly depends on the Finite Element mesh used in the numerical inversion procedure (see Borsic *et al.* 2005). As for test B, no evident cracks were detected through visual inspection or ERT monitoring.

The water content increased quickly during the water uptake stage, although in both tests it did not recover its initial value. Interestingly, errors in the electrical measurements decreased with water uptake and the estimate of the average water content based on the ERT matched again very well with the physical one (Figure 6).

Figure 9 shows the evolution with the water content of the tip resistance detected with the pocket penetrometer on the samples matrix. For both curing times, the tip resistance increases as the water content decreases, i.e. as the mixture desaturates and suction increases. At any water content, the resistance of the test B is higher than the one of the test A, which might contribute explaining why significant cracks did not develop during test B.

Some complementary Unconsolidated Undrained triaxial tests were carried out on specimens cured for 28 and 60 days. The uniaxial compressive strength was 38 kPa after 28 days and 100 kPa after

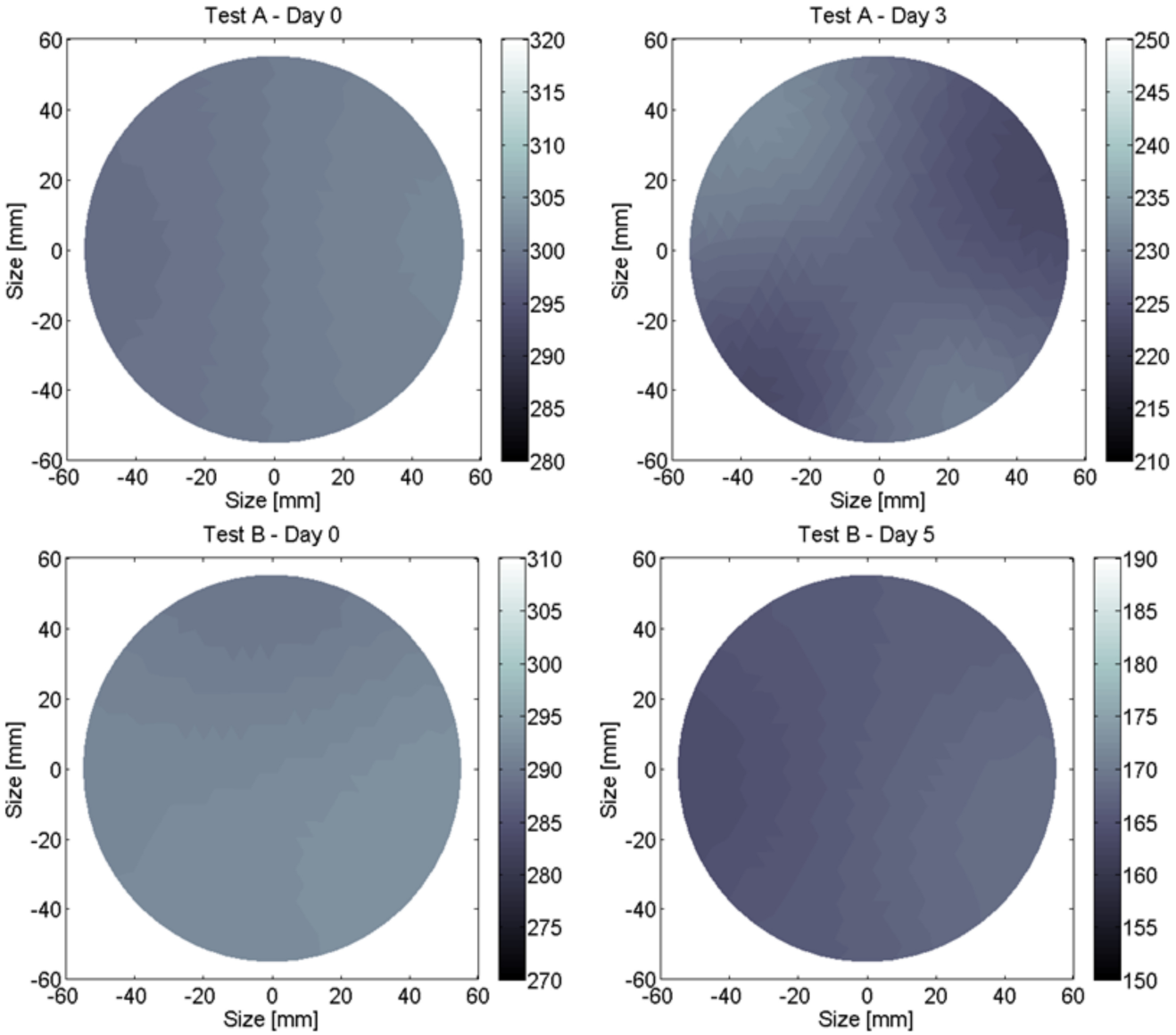

Figure 7: ERT reconstructed water content distribution during drying. Colorbars are gravimetric water contents in %

60 days. Compared with Figure 8, these results suggest that the pocket penetrometer measurements provide a rough estimation of the uniaxial compressive strength, as also pointed out in the literature (see *e.g.* Blum 1997). The uniaxial compressive strength after one month of curing was also roughly comparable to the one obtained on a similar mixture for the same curing time by Evans and Opdyke (2006).

4.2 Column sample

The main purpose of the column test was to observe local evolutions of the water content during drying and water uptake, also detecting the possible development of cracks. Relying on the results obtained with the squat samples, arrays of electrodes were disposed at three different heigths from

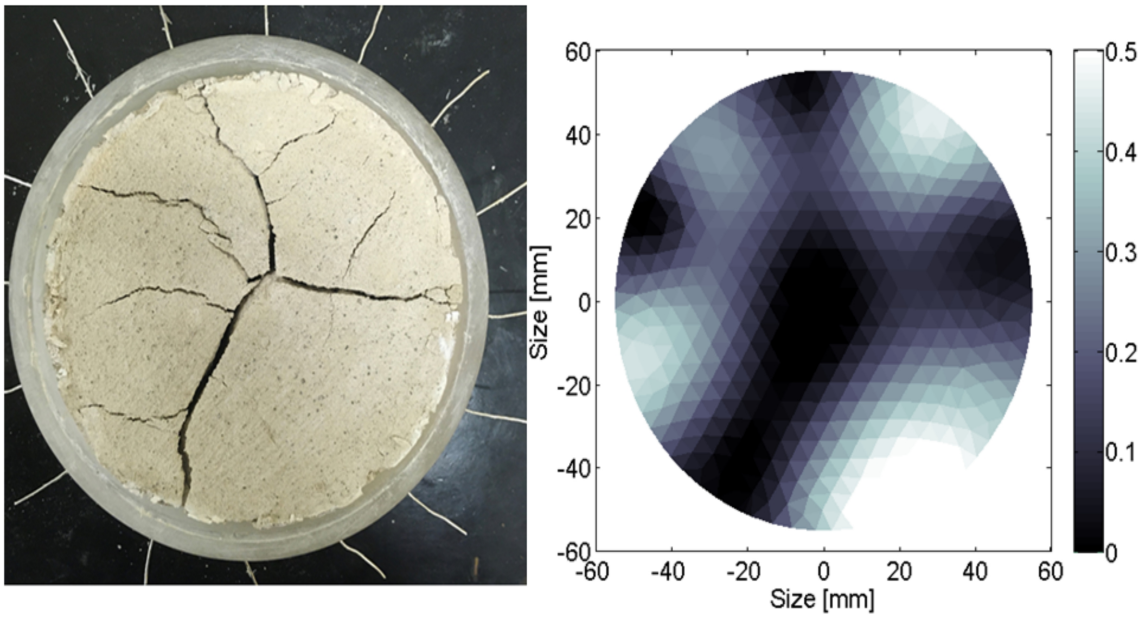

Figure 8: Picture of test A sample sample after 10 days of drying (left) and corresponding map of electrical conductivity (right, values in mS/cm).

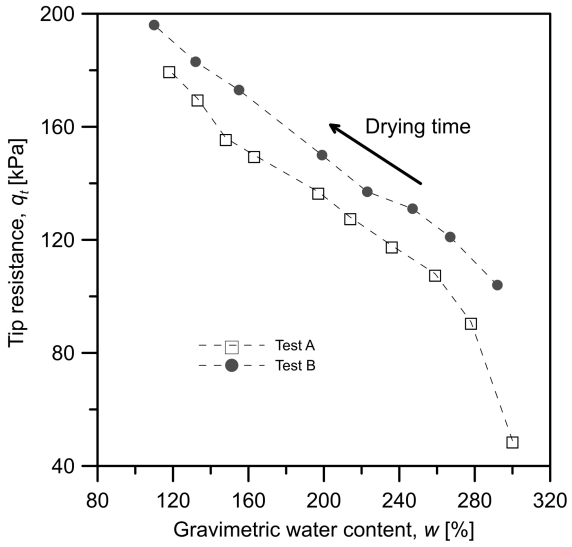

Figure 9: Relationship between water content and tip resistance from pocket penetrometer measurements

the bottom of the column (respectively z_1=75 mm, z_2=150 mm and z_3=225 mm) to run ERT reconstructions from which local evaluations of the water content in time were deduced. The void ratio of this sample, determined through mass measurements, varied with depth and it was e = 6.60 at the bottom and e = 8.50 at its top. Such variation is likely to be due to the self-weight induced consolidation taking place during curing,

Figure 10 shows the evolution with time of the water content at the monitored points. Higher water contents pertain to the upper layers, which have a larger void ratio. The ERT results suggest a limited loss of water mass during the 13 days of drying (stage 1): the largest decrease in water content

corresponded to z_3 ($\Delta w \simeq 40$ %) whereas the smallest corresponded to z_1 ($\Delta w \simeq 25$ %). As already detected with the squat samples, with the water uptake the water content increased, but it did not fully recover its initial value. This was surely due to the irreversible reduction in the void ratio and to the development of microcracks along drying as described in Section 3. A further contribution could come from the persistence of air bubbles, providing an irreducible air saturation at the pressure given by the limited water height imposed at sample bottom. The water content increased well within 60 minutes from the beginning of the imbibition stage and then remained about constant.

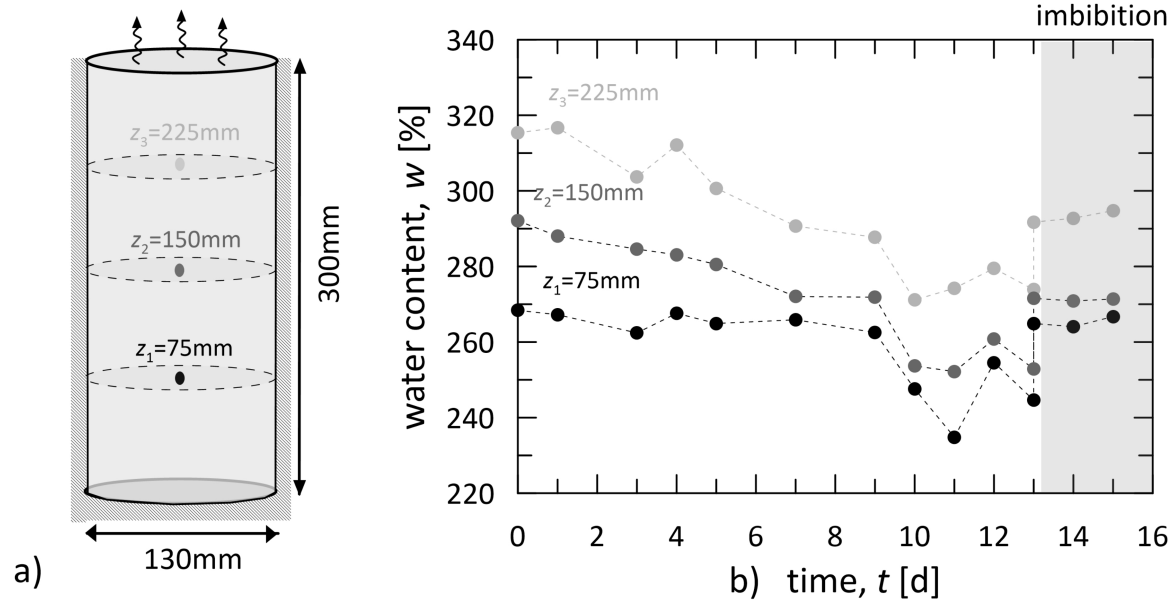

Figure 10: Results of the evaporation and water uptake bench scale test: trends with time of the water content along the column sample as evaluated by ERT

5 Modelling of evaporation and water uptake

Numerical simulations were run to achieve a further understanding of the evaporation and water uptake processes. The balance of water mass as a chemical species and of the thermal energy of the mixture in unsaturated conditions were implemented and solved with the Finite Element commercial code Comsol Multiphysics ®. 1D models were set up to reproduce the laboratory tests discussed in the previous sections. A full description of the Thermo-Hydraulic (TH) model and of the related equations is provided in the Appendix. A continuum approach was adopted, *i.e.* the presence of fractures was not introduced. Changes in porosity with suction were accounted for introducing an empirical equation based on the results presented in figure 3. The hydraulic parameters obtained from the experimental results described in Section 3 were used, together with the van Genuchten relationship for relative permeability function and a linear scanning equation $dS_l = -k_s ds$ with

$k_s = 4 \cdot 10^{-5}$ 1/kPa for the transition from the main wetting to the main drying retention curve. Thermal parameters were estimated using relationships from the literature accounting for the properties of the single phases.

The initial and boundary conditions for the balance equations of water mass and energy, summarised in Table 3, were chosen to reproduce laboratory conditions. A hydrostatic water pressure distribution and a uniform temperature, equal to the laboratory one $T = 21°C$, were adopted as initial conditions. The hydraulic and heat fluxes induced by evaporation and briefly discussed in the following (Eqs.6 and 9, respectively) were imposed at the top boundary. At the bottom boundary either a no hydraulic flow or a water pressure corresponding to the imposed water height h_w were imposed, so to reproduce the drying and the water uptake stage respectively. A constant temperature of $T_{amb} = 21°$C was applied for both stages.

Table 3: Initial and boundary conditions

	Water mass balance	Energy balance
Initial conditions		
$t = 0$	$u_w = \rho_w g(z-h)$	$T = T_{amb}$
Boundary conditions: evaporation stage		
top ($z = h$)	evaporative flux Eq.(6)	heat flux Eq.(9)
bottom ($z = 0$)	no flux	$T = T_{amb}$
Boundary conditions: imbibition stage		
top ($z = h$)	evaporative flux Eq.(6)	heat flux Eq.(9)
bottom ($z = 0$)	$u_w = \rho_w g h_w$	$T = T_{amb}$

The outflow of water mass q_{evap} due to evaporation was evaluated as a function of the actual rate of evaporation AE, defined as (Penman, 1956):

$$q_{evap} = \rho_l AE; \qquad AE = PE \frac{p_{v,soil} - p_{v,amb}}{p_{v,sat} - p_{v,amb}}; \tag{6}$$

where ρ_l is the water mass density, PE is the potential rate of evaporation, $p_{v,soil} = p_{v,sat}(T)h_r(T_{soil})$ is the current vapour pressure in the soil at soil temperature T_{soil}, $p_{v,amb} = p_{v,sat}(T_{amb})h_r(T_{amb})$ is the vapour pressure in the environment, and $p_{v,sat}$ is the saturated vapour pressure, related to temperature according to Kendall and Caldwell (1998)

$$p_{v,sat}[\text{kPa}] = 0.6108 \cdot 10^{\frac{7.5(T[°\text{C}]-273.15)}{T[°\text{C}]}}. \tag{7}$$

while the relative humidity is linked to total suction ψ through the psychrometric law (8):

$$h_r = \exp\left(-\frac{\psi M_w}{\rho_l R T}\right), \tag{8}$$

where M_w is the molar mass of the water, R is the constant of perfect gases.

In testing conditions, PE was determined placing a mold filled of water in the laboratory environment for seven days and monitoring its weight loss in time with a balance. The measured potential evaporation was $PE = 2.58$ mm/d.

Due to the thermo-hydraulic coupling, the evaporation process also acts as a heat sink that causes a reduction of temperature. On the other hand, the difference of temperature between the soil and the environment generates a heat flux which aims at re-establishing equilibrium. The thermal flux that was imposed at the upper boundary, subjected to evaporation, was thus (Ralaizafisoloarivony *et al.*, 2020):

$$q_{heat} = -L_w q_{evap} + \epsilon_s \sigma (T_{amb}^4 - T^4); \tag{9}$$

where L_w is the latent heat of vaporization, $\epsilon_s = 0.9 + 0.18w$ is soil emissivity, linked with gravimetric water content w according to Van Bavel and Hillel (1976), and $\sigma = 5.670367 \cdot 10^{-8}$ kg s^{-3}K^{-4} is Stefan-Boltzmann constant.

5.1 Squat samples

Figure 11 shows the model predictions in terms of evolution of the hydraulic state at centre of the squat samples (height 20 mm). At the end of the drying stage, the predicted average degree of saturation for the two samples is around $S_l = 0.3$ and 0.5 respectively (see Figure 11.a), thus far from the residual degree of saturation. When the imbibition begins, suction starts to decrease due to the imposed water head at the bottom boundary, and the samples increase their water content in accordance to the scanning retention path shown in Figure 11. The scanning path of the water retention curve is followed until reaching the main wetting branch.

Figure 12 reports the predicted evolution of the average water content with time, compared with experimental data. Model predictions are satisfactory and in the simulations the initial water content was not completely recovered after the imbibition phase being the final degree of saturation lower than 1. The variation of the void ratio due to the shrinkage induced by drying is not affecting much the hydraulic behaviour of the material, as the maximum values of suctions achieved are around 5 MPa (see Figure 11), that corresponds -according to Figure 2- to a negligible void ratio change.

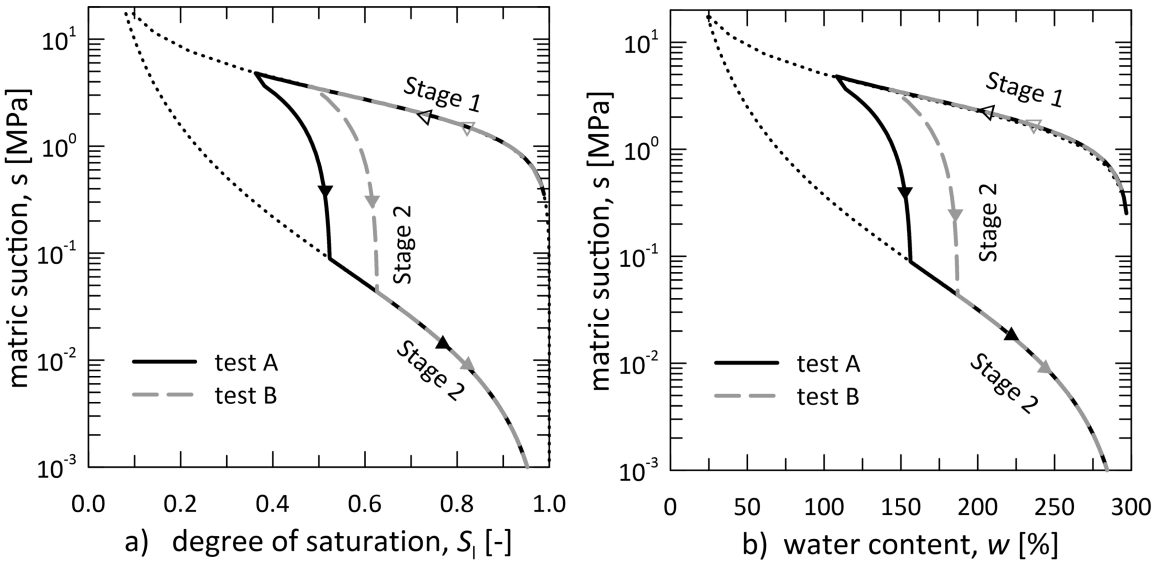

Figure 11: Drying and water uptake paths at the centre of the squat samples a) in the degree of saturation -suction plane; b) in the water content -suction plane

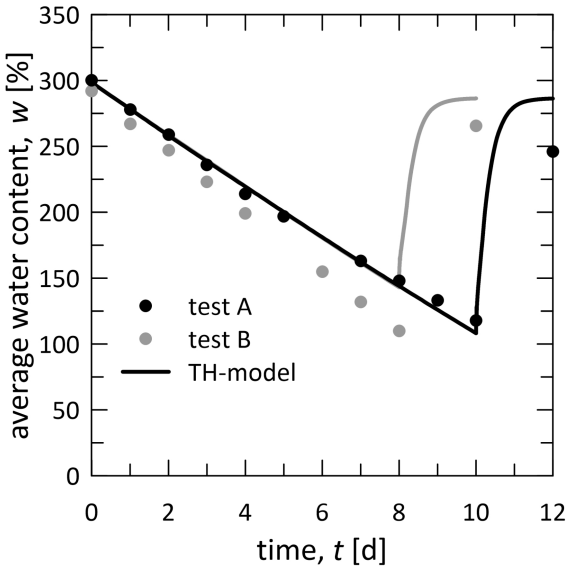

Figure 12: Average water content with time: models prediction *versus* experimental data

However, the analysis slightly overestimates the final water content. This seems to suggest that mass of water retained along the main wetting path at low suctions is less than what predicted through eq. 5, being the parameter reported in Table 1 determined at suctions $s > 50$ kPa.

5.2 Column sample

Figure 13 compares the predicted and the experimental evolution of water content at the column monitoring points. A quite good match between the experimental data and the simulations is found, although the model anticipates and slightly overestimates the decrease in water content in correspondence of z_1. The partial recovery of water content caused by the water uptake is nicely repro-

duced, both in terms of water amount and of time evolution.

Figure 14 shows the predicted hydraulic paths: suction values at the different depths are quite homogeneous, and the differences in the water content is predominantly due to the depth-dependency of the initial void ratio. At the end of the drying stage, suction ranges around 1 MPa and the sample is very far from full desaturation, so that the water uptake stage is governed by the scanning water retention curve path, that allows the sample to recover about the 20% of water content.

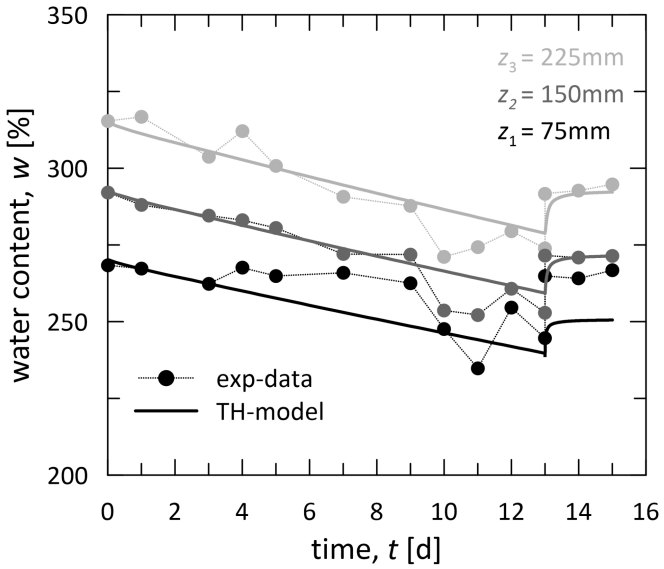

Figure 13: a) Evolution in time of the water content in the column sample. Model predictions *versus* experimental data.

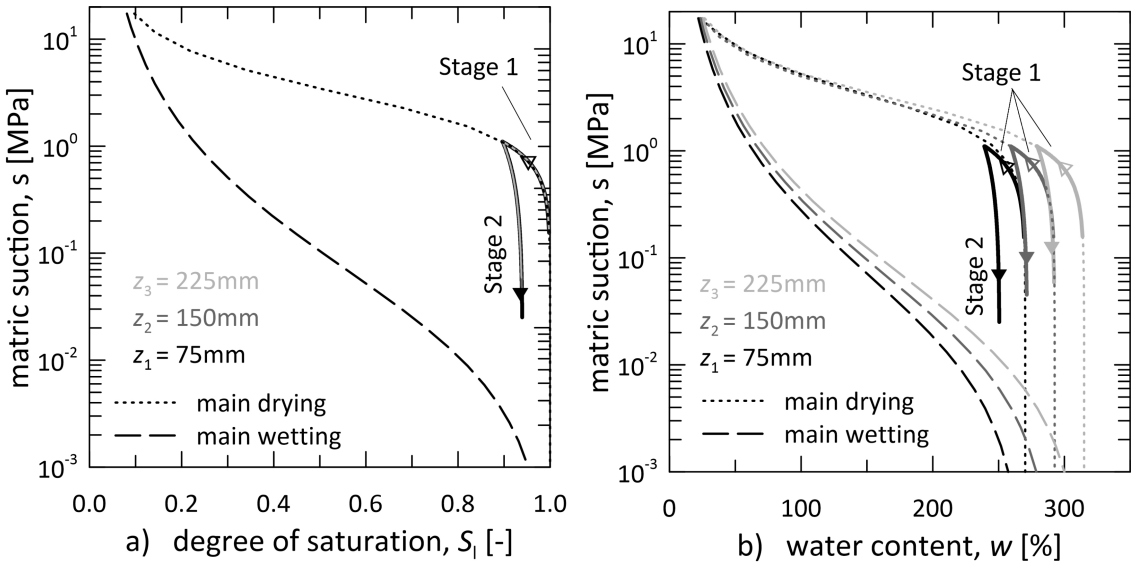

Figure 14: Drying and water uptake paths of the column test a) in the degree of saturation -suction plane; b) in the water content -suction plane.

6 Conclusions

The results of this laboratory investigation allow drawing some conclusions on the behaviour of a CB mixture upon drying and wetting. Although the water retention properties along the main drying path were quite good, with an Air Entry Value of around 800 kPa, a large hydraulic hysteresis was found and the main wetting curve had significantly lower retention capabilities. According to SEM evidence, this might be due to the retraction of cement-bentonite clusters, which leads to the opening of small microcracks: these are well evident at a threshold suction of about 4 MPa and they still enlarge as drying proceeds. Retraction might be only partially reversible, as it is also confirmed by the plastic volumetric strains that develop once that the mixture is exposed to high suctions.

In the laboratory environment, evaporation was able to cause an appreciable water content decrease only when the bottom of squat and column samples was sealed (*i.e.* no water recharge was made available). In this case, the mixtures dried. Cracking of squat samples upon drying occurred above a suction of about 4 MPa for samples cured for 28 days days, while it was not evident over the same range of suctions for samples cured for 60 days. A possible reason for this difference might be the increase of the material strength with the curing time. Tests were also monitored with Electrical Resistivity Tomography (ERT), which proved to be effective in determining the water content of the mixture at relatively high water contents. Although at lower water content ERT estimates might be erroneous, it can still provide a reasonable detection of crack patterns when they arise, which suggests that ERT might be fruitfully used for on-site integrity inspections.

Results of an evaporation and water uptake bench scale test on a CB column showed that, while water loss occurs at a relatively slow pace, water uptake occurs in very short time. The initial water content was not recovered in any test, even if the samples had experienced relatively modest suctions (order of a few MPas). For all the laboratory experiments, the transient processes of evaporation process and water uptake were adequately reproduced by continuous models accounting for water and heat transport in unsaturated state, which were built upon the material properties deduced from water retention and permeability testing.

Field evidences discussed in the introduction (Jefferis, 2012; Soga *et al.*, 2013) are inconclusive with respect to the question whether cement-bentonite cutoff walls might crack or not during their service life. The experimental results of this study suggest that, besides on the mechanical constraints acting in situ, this is clearly related to the suction acting in the barrier. On its turn, suction in the wall would not only depend on the interaction with the atmosphere of the site, but also on the amount of water made available by the surrounding soils. In fact, in the experimental data shown in the paper

water content changes were very small when a free drainage condition was imposed at the bottom of the column sample, while they were more pronounced when the bottom was sealed. The methodology here presented (water retention and mechanical characterization, modelling based on mass and energy balance equations) could help the practitioners to identify the risk of cracking accounting for the actual stratigraphy and the environmental conditions of the site. In this case, however, the definition of the soil-atmosphere boundary conditions should be updated to account for environmental features such as wind velocity, solar radiations, daily and seasonal variation of temperature and relative humidity.

Acknowledgements

Tests on squat and column samples were run by A. Zibisco, whose contribution is gratefully acknowledged. The activity of one of Dr. Giulia Guida was financed in the context of the public administration agreement between Politecnico di Milano - Department of Civil and Environmental Engineering and the Italian Ministry of Economic Development, Direzione Generale per la Sicurezza anche Ambientale delle Attività Minerarie ed Energetiche–Ufficio Nazionale Minerario per gli Idrocarburi e le Georisorse–Programme Clypea, which is here gratefully acknowledged.

References

An, N., Hemmati, S., Cui, Y.-j. and Tang, C.-s. (2018), 'Numerical investigation of water evaporation from fontainebleau sand in an environmental chamber', *Engineering Geology* **234**, 55–64.

ASTM (2016), *ASTM D5298-2016*, ASTM International.

Blum, P. (1997), 'Physical properties handbook: a guide to the shipboard measurement of physical properties of deep-sea cores', *ODP Tech. Note* **26**.

Borsic, A., Comina, C., Foti, S., Lancellotta, R. and Musso, G. (2005), 'Imaging heterogeneities with electrical impedance tomography: laboratory results', *Géotechnique* **55**(7), 539–547.

Cao, B., Chen, J. and Al-Tabbaa, A. (2021), 'Crack-resistant cement–bentonite cut-off wall materials incorporating superabsorbent polymers', *Canadian Geotechnical Journal* **58**(6), 800–810.

Cermak, J., Evans, J. and Tamaro, G. J. (2012), Evaluation of soil-cement-bentonite wall performance-effects of backfill shrinkage, *in* 'Grouting and Deep Mixing 2012: Proceedings of the Fourth Inter-

national Conference on Grouting and Deep Mixing, February 15-18, 2012. New Orleans, Lousiana, United States', pp. 502–511.

Comina, C., Cosentini, R. M., Della Vecchia, G., Foti, S. and Musso, G. (2011), '3d-electrical resistivity tomography monitoring of salt transport in homogeneous and layered soil samples', *Acta Geotechnica* **6**(4), 195–203.

Cosentini, R. M., Della Vecchia, G., Foti, S. and Musso, G. (2012), 'Estimation of the hydraulic parameters of unsaturated samples by electrical resistivity tomography', *Géotechnique* **62**(7), 583–594.

Cosenza, P., Guerin, R. and Tabbagh, A. (2003), 'Relationship between thermal conductivity and water content of soils using numerical modelling', *European Journal of Soil Science* **54**(3), 581–588.

Delage, P. and Pellerin, F. (1984), 'Influence de la lyophilisation sur la structure d'une argile sensible du Québec', *Clay minerals* **19**(2), 151–160.

Evans, J. C. (1994), Hydraulic conductivity of vertical cutoff walls, *in* 'Hydraulic conductivity and waste contaminant transport in soil, ASTM Special Technical Publication', Vol. 1142, American Technical Publisher LTD, pp. 79–79.

Evans, J. C. and Opdyke, S. M. (2006), Strength, permeability, and compatibility of slag-cement-bentonite slurry wall mixtures for constructing vertical barriers, *in* '5th ICEG Environmental Geotechnics: Opportunities, Challenges and Responsibilities for Environmental Geotechnics: Proceedings of the ISSMGE's fifth international congress organized by the Geoenvironmental Research Centre, Cardiff University and held at Cardiff City Hall on 26–30th June 2006', Thomas Telford Publishing, pp. 118–125.

Evans, J. and Ruffing, D. (2017), Design and construction of an experimental soil-bentonite cutoff wall, *in* 'ASCE Geotechnical Frontiers 2017, March 12-15, 2017. Orlando, Florida', pp. 164–174.

Flessati, L., Della Vecchia, G. and Musso, G. (2021), 'Mechanical behavior and constitutive modeling of cement–bentonite mixtures for cutoff walls', *Journal of Materials in Civil Engineering* **33**(3), 04020483.

Fratalocchi, E., Pasqualini, E. and Balboni, P. (2006), Performance of a cement-bentonite cut-off wall in an acidic sulphate environment, *in* '5th ICEG Environmental Geotechnics: Opportunities, Challenges and Responsibilities for Environmental Geotechnics: Proceedings of the ISSMGE's fifth in-

ternational congress organized by the Geoenvironmental Research Centre, Cardiff University and held at Cardiff City Hall on 26–30th June 2006', Thomas Telford Publishing, pp. 133–139.

Guida, G., Musso, G., Sanetti, G., di Prisco, C. and Della Vecchia, G. (2021), 'A procedure to estimate cutoff wall transport properties from monitoring wells', *International Journal for Numerical and Analytical Methods in Geomechanics* **45**(9), 1282–1299.

Hilf, J. W. (1956), *An investigation of pore-water pressure in compacted cohesive soils*, Ph.D Thesis, University of Colorado at Boulder.

Jefferis, S. (2012), Cement-bentonite slurry systems, *in* 'Grouting and Deep Mixing 2012: Proceedings of the Fourth International Conference on Grouting and Deep Mixing, February 15-18, 2012. New Orleans, Lousiana, United States', pp. 1–24.

Joshi, K., Soga, K. and Tedd, P. (2009), Long-term performance of cement-bentonite containment wall, *in* 'Proceedings of the 17th International Conference on Soil Mechanics and Geotechnical Engineering (Volumes 1, 2, 3 and 4)', IOS Press, pp. 2028–2031.

Kendall, C. and Caldwell, E. A. (1998), Fundamentals of isotope geochemistry, *in* 'Isotope tracers in catchment hydrology', Elsevier, pp. 51–86.

Kimball, B. A., Jackson, R., Reginato, R., Nakayama, F. and Idso, S. (1976), 'Comparison of field-measured and calculated soil-heat fluxes', *Soil Science Society of America Journal* **40**(1), 18–25.

Lai, S.-H., Tiedje, J. M. and Erickson, A. E. (1976), 'In situ measurement of gas diffusion coefficient in soils', *Soil Science Society of America Journal* **40**(1), 3–6.

Malusis, M. A., Evans, J. C., Jacob, R. W., Ruffing, D., Barlow, L. and Marchiori, A. M. (2017), Construction and monitoring of an instrumented soil-bentonite cutoff wall: field research case study, *in* 'Proceedings of the 29th Central Pennsylvania Geotechnical Conference, Hershey, PA, USA', Vol. 31.

Malusis, M. A., Yeom, S. and Evans, J. C. (2011), 'Hydraulic conductivity of model soil–bentonite backfills subjected to wet–dry cycling', *Canadian Geotechnical Journal* **48**(8), 1198–1211.

Musso, G., Zibisco, A., Cosentini, R. M., Trischitta, P. and Della Vecchia, G. (2020), Monitoring drying and wetting of a cement bentonite mixture with electrical resistivity tomography, *in* 'E3S Web of Conferences', Vol. 195, EDP Sciences, p. 03015.

Penman, H. L. (1956), 'Estimating evaporation', *Eos, Transactions American Geophysical Union* **37**(1), 43–50.

Ralaizafisoloarivony, N., Tran, K., Degré, A., Mercatoris, B., Léonard, A., Toye, D. and Charlier, R. (2020), Experimental and numerical investigation of the drying of an agricultural soil, *in* 'E3S Web of Conferences', Vol. 195, EDP Sciences, p. 01034.

Royal, A., Opukumo, A., Qadr, C., Perkins, L. and Walenna, M. (2018), 'Deformation and compression behaviour of a cement–bentonite slurry for groundwater control applications', *Geotechnical and Geological Engineering* **36**(2), 835–853.

Ryan, C. (1985), 'Slurry cutoff walls: Applications in the control of hazardous wastes', *ASTM special technical publication* (874), 9–22.

Saito, H., Simunek, J. and Mohanty, B. P. (2006), 'Numerical analysis of coupled water, vapor, and heat transport in the vadose zone', *Vadose Zone Journal* **5**, 784–800.

Sarsby, R. W. (2013), Tailings dams, *in* 'Environmental geotechnics', ICE Publishing, pp. 365–391.

Shokri, N., Lehmann, P. and Or, D. (2010), 'Evaporation from layered porous media', *Journal of Geophysical Research: Solid Earth* **115**(B6).

Smyl, D., Hallaji, M., Seppänen, A. and Pour-Ghaz, M. (2016), 'Quantitative electrical imaging of three-dimensional moisture flow in cement-based materials', *International Journal of Heat and Mass Transfer* **103**, 1348–1358.

Smyl, D., Rashetnia, R., Seppänen, A. and Pour-Ghaz, M. (2017), 'Can electrical resistance tomography be used for imaging unsaturated moisture flow in cement-based materials with discrete cracks?', *Cement and Concrete Research* **91**, 61–72.

Soga, K., Joshi, K. and Evans, J. (2013), 'Cement bentonite cutoff walls for polluted sites', *Coupled Phenomena in Environmental Geotechnics* p. 149.

Trischitta, P., Cosentini, R. M., Della Vecchia, G., Sanetti, G. and Musso, G. (2020), Preliminary investigation on the water retention behaviour of cement bentonite mixtures, *in* 'E3S Web of Conferences', Vol. 195, EDP Sciences, p. 03032.

Van Bavel, C. and Hillel, D. (1976), 'Calculating potential and actual evaporation from a bare soil surface by simulation of concurrent flow of water and heat', *Agricultural Meteorology* **17**(6), 453–476.

Vespo, V. S., Della Vecchia, G. and Musso, G. (2020), Modelling evaporation processes of cement-bentonite mixtures, *in* 'E3S Web of Conferences', Vol. 195, p. 02029.

Wilson, G. W. (1990), *Soil evaporative fluxes for geotechnical engineering problems*, Ph.D Thesis, University of Saskatchewan Saskatoon.

Wu, H.-l., Jin, F. and Du, Y.-j. (2019), 'Influence of wet-dry cycles on vertical cutoff walls made of reactive magnesia-slag-bentonite-soil mixtures', *Journal of Zhejiang University-SCIENCE A* **20**(12), 948–960.

Zibisco, A. (2019), *Messa in sicurezza permanente di siti contaminati da idrocarburi leggeri: studio del processo di desaturazione di miscele cemento-bentonite tramite tecnica ERT*, Ph.D Thesis, Politecnico di Torino.

Appendix: Formulation of the Thermo-Hydraulic model for the drying and water uptake problem

Evaporation is a complex process involving simultaneous heat and mass transfer, phase changes, and inter-facial liquid and vapour transfer at pore scales (Saito *et al.*, 2006; Shokri *et al.*, 2010; An *et al.*, 2018). Pore water chemistry and material deformation can play a relevant role too, despite in many application a set of equations including just the coupled transient movement of liquid water, water vapour, and heat in the soil is sufficient (Wilson, 1990). In this work, evaporation was simulated by integrating the coupled water mass balance and the mixture energy balance equation (Thermo-Hydraulic model, T-H). Changes in porosity were accounted for in both balance equations, accordingly with the suction-void ratio relationship of Figure 3.

Water mass balance

It is well recognized that during evaporation processes water may flow to the ground surface as both liquid water and water vapour. If fluid phases are accounted for, molecules of water and dissolved air compose the liquid phase, while molecules of dry air and water vapour compose the gas phase. Trough evaporation, molecules of water are exchanged between the liquid and the gas phase. In order to avoid modelling the transfer of mass between the two phases and the mass balance of the dry air, water liquid and vapour, the mass balance equation was simply imposed on water as a chemical species as:

$$\frac{\partial}{\partial t}\left[\phi(S_l c_l^w + S_g c_g^w)\right] + \nabla\cdot\left(c_l^w \mathbf{q}_l + c_g^w \mathbf{q}_g\right) + \nabla\cdot\phi\left(S_l \mathbf{J}_l^w + S_g \mathbf{J}_g^w\right) = S_l\phi\rho_l\Gamma_l^w + S_g\phi\rho_g\Gamma_g^w \qquad (10)$$

where ϕ is porosity, S_l and S_g are the degree of saturation of the liquid and the gas phase respectively ($S_l + S_g = 1$), c_l^w and c_g^w are the water mass concentration in the liquid and gas phase, ρ_l and ρ_g are the liquid and gas mass density, $\mathbf{q}_l$ and $\mathbf{q}_g$ are the advective fluxes of the liquid and gas phase, $\mathbf{J}_l^w$ and $\mathbf{J}_g^w$ are the sum of diffusive and dispersive fluxes of water in liquid and gas phase, Γ_l^w and Γ_g^w are the generation rate of water mass per unit mass of liquid and gas phase. For the simulation of evaporation processes, it was accepted that the water mass balance equation may be simplified by neglecting the source terms, the dispersive flux of water vapour, the presence of air dissolved in the liquid (which implies $c_l^w = \rho_l$, considered constant throughout the paper, and $\mathbf{J}_l^w = 0$) and by assuming that air pressure is constant over space and time (which implies $\mathbf{q}_g = 0$). It follows that:

$$\frac{\partial}{\partial t}\left[\phi(S_l\rho_l + S_g c_g^w)\right] + \nabla\cdot\left(\rho_l \mathbf{q}_l\right) + \nabla\cdot\phi\left(S_g \mathbf{J}_g^w\right) = 0. \tag{11}$$

The specific discharge of liquid water $\mathbf{q}_l$ in the unsaturated material was expressed by means of a generalized Darcy law as

$$\mathbf{q}_l = -\frac{\mathbf{K}_w(S_l)}{\rho_l g}\nabla(u_l + \rho_l g z), \tag{12}$$

where $\mathbf{K}_w$ is the unsaturated hydraulic conductivity, g is the gravitational acceleration, u_l is the liquid water pressure and z is the elevation head. The unsaturated hydraulic conductivity was estimated as the product between the saturated one $\mathbf{K}_w^{sat}$ and the relative permeability coefficient k_r, which in turn was set to depend on water degree of saturation according to the van Genuchten equation

$$\mathbf{K}_w = \mathbf{K}_w^{sat}\cdot k_r = \mathbf{K}_w^{sat}\cdot S_e^{0.5}\left[1-\left(1-S_e^{1/m}\right)^m\right]^2, \tag{13}$$

being $S_e = \frac{S_l - S_{res}}{1-S_{res}}$ the effective water degree of saturation, S_{res} the residual degree of saturation and m a material parameter.

The diffusive flux of water vapour in the unsaturated material was expressed through Fick's law as

$$\mathbf{J}_g^w = -\mathbf{D}(S_g)\nabla c_g^w, \tag{14}$$

where $\mathbf{D} = D_v\boldsymbol{\tau}(S_g)$ is the water vapour diffusion tensor of the porous medium, that was set equal to the product of the diffusion coefficient of vapour in free air D_v and the tortuosity tensor $\boldsymbol{\tau}(S_g)$, which accounts for the tortuosity of the path of water vapour molecules through the porous medium. Following Lai *et al.* (1976), it was assumed $\tau = \left(\phi S_g\right)^{2/3}$. The vapour diffusivity coefficient in free air depends in turns on temperature, $D_v[\mathrm{m}^2/\mathrm{s}] = 0.229\cdot 10^{-4}(1+T[\mathrm{K}]/273)^{1.75}$ (Kimball *et al.*, 1976).

The relation between the degree of saturation of the liquid phase S_l and matric suction $s = u_g - u_l$ is given by the water retention curve, that in this work was expressed by means of the van Genuchten equation (5), with parameters provided in Table 1.

Vapour concentration c_g^w is *viceversa* related to the relative humidity h_r (Eq.8), and then on total suction ψ via the psychometric law:

$$c_g^w = c_{g,sat}^w h_r, \tag{15}$$

where $c_{g,sat}^w$ is the saturated concentration of water vapour. The ideal gas law allows the evaluation

of $c^w_{g,sat}$ as a function the saturated vapour pressure of water vapour $p_{v,sat}$:

$$c^w_{g,sat} = \frac{p_{v,sat} M_w}{RT}. \tag{16}$$

Finally, the saturated vapour pressure can be linked with temperature according to Kendall and Caldwell (1998)(7). Under the assumptions that osmotic suction is constant over time and space and the variation of the gas phase pressure is negligible compared to that of the liquid phase, changes in total and matric suction are equal and about opposite to changes in water pressure, $\Delta s = \Delta\psi \approx -\Delta u_l$.

Energy balance

The energy balance equation through porous medium can be expressed as (17):

$$\frac{\partial}{\partial t}\left(E_s\rho_s(1-\phi) + E_l\rho_l S_l\phi + E_g\rho_g S_g\phi\right) + \nabla\cdot\left(\mathbf{i}_c + \mathbf{j}_{E_s} + \mathbf{j}_{E_l} + \mathbf{j}_{E_g}\right) = 0, \tag{17}$$

where $E_s = c_{p,s}T$, $E_l = c_{p,l}T$, $E_g = c_{p,v}T + L_w$ represent the energy stored at temperature T in the solid, in the liquid and in the gas phase, respectively, and they depends on the corresponding specific heat capacity ($c_{p,s}, c_{p,l}, c_{p,v}$) and on the latent heat of vaporization L_w. The specific heat capacity adopted for the cement bentonite solid (Vespo *et al.*, 2020), liquid and gaseous phase are respectively $c_{p,s}$ = 1107 J/(kg K), $c_{p,w}$ = 4182 J/(kg K), $c_{p,v}$ = 2062 J/(kg K). The conduction of sensible heat is accounted for via the term $\mathbf{i}_c$, that can be linearly linked to the gradient of temperature via the Fourier law

$$\mathbf{i}_c = -\lambda\nabla T \tag{18}$$

where λ is the thermal conductivity of the medium, that was evaluated according to Cosenza *et al.* (2003) as a function of the different phase contributions: $\lambda = \left(\theta_s\sqrt{\lambda_s} + \theta_w\sqrt{\lambda_w} + \theta_v\sqrt{\lambda_v}\right)^2$, where λ_s = 1.345 W/(m K), λ_w = 0.6 W/(m K), λ_v = 0.024 W/(m K) are the thermal conductivity of the solid, water and vapour phase respectively. Energy flux related to the movement of the three phases was evaluated as follows:

$$\begin{aligned}
\mathbf{j}_{E_s} &= 0 \\
\mathbf{j}_{E_l} &= E_l\mathbf{q}_l = c_{p,l}T\left[-\frac{\mathbf{K}^{sat}_w k_r}{g}\nabla(u_w + \rho_l g z)\right] \\
\mathbf{j}_{E_g} &= E_g\mathbf{J}^w_g = (c_{p,v}T + L_w)\left[-\phi(1-S_l)D_v\tau\frac{c^w_g M_w}{\rho_l RT}\left(\nabla u_l - \frac{u_l}{T}\nabla T\right)\right].
\end{aligned} \tag{19}$$